



















REPORT

OPEN ACCESS



Novel super-neutralizing antibody UT28K is capable of protecting against infection from a wide variety of SARS-CoV-2 variants

Tatsuhiko Ozawa ^{a,#}, Hideki Tani ^{b,#}, Yuki Anraku ^{c,#}, Shunsuke Kita ^c, Emiko Igarashi^b, Yumiko Saga^b, Noriko Inasaki^b, Hitoshi Kawasuji^d, Hiroshi Yamada ^e, so-Ichiro Sasaki^f, Mayu Somekawa ^e, Jiei Sasaki^g, Yoshihiro Hayakawa ^f, Yoshihiro Yamamoto ^d, Yoshitomo Morinaga ^e, Nobuyuki Kurosawa ^h, Masaharu Isoe ^h, Hideo Fukuhara ^c, Katsumi Maenaka ^c, Takao Hashiguchi ^g, Hiroyuki Kishi ^a, Isao Kitajima ⁱ, Shigeru Saito ⁱ, and Hideki Niimi ⁱ

^aDepartment of Immunology, Faculty of Medicine, Academic Assembly, University of Toyama, Toyama, Japan; ^bDepartment of Virology, Toyama Institute of Health, Toyama, Japan; ^cFaculty of Pharmaceutical Sciences, Hokkaido University, Sapporo, Japan; ^dDepartment of Clinical Infectious Diseases, Faculty of Medicine, Academic Assembly, University of Toyama, Toyama, Japan; ^eDepartment of Microbiology, Faculty of Medicine, Academic Assembly, University of Toyama, Toyama, Japan; ^fSection of Host Defences, Department of Bioscience, Institute of Natural Medicine, University of Toyama, Japan; ^gLaboratory of Medical Virology, Institute for Frontier Life and Medical Sciences, Kyoto University, Kyoto, Japan; ^hDepartment of Life Sciences and Bioengineering, Laboratory of Molecular and Cellular Biology, Faculty of Engineering, Academic Assembly, University of Toyama, Toyama, Japan; ⁱAdministrative office, University of Toyama, Toyama, Japan; ^jDepartment of Clinical Laboratory and Molecular Pathology, Faculty of Medicine, Academic Assembly, University of Toyama, Toyama, Japan

ABSTRACT

Many potent neutralizing SARS-CoV-2 antibodies have been developed and used for therapies. However, the effectiveness of many antibodies has been reduced against recently emerging SARS-CoV-2 variants, especially the Omicron variant. We identified a highly potent SARS-CoV-2 neutralizing antibody, UT28K, in COVID-19 convalescent individuals who recovered from a severe condition. UT28K showed efficacy in neutralizing SARS-CoV-2 in an *in vitro* assay and *in vivo* prophylactic treatment, and the reactivity to the Omicron strain was reduced. The structural analyses revealed that antibody UT28K Fab and SARS-CoV-2 RBD protein interactions were mainly chain-dominated antigen-antibody interactions. In addition, a mutation analysis suggested that the emergence of a UT28K neutralization-resistant SARS-CoV-2 variant was unlikely, as this variant would likely lose its competitive advantage over circulating SARS-CoV-2. Our data suggest that UT28K offers potent protection against SARS-CoV-2, including newly emerging variants.

ARTICLE HISTORY

Received 20 March 2022
Revised 17 April 2022
Accepted 27 April 2022

KEYWORDS

COVID-19; SARS-CoV-2; neutralizing antibody; monoclonal antibody; super-neutralizing antibody





Introduction

Severe acute respiratory syndrome coronavirus 2 (SARS-CoV-2) is the etiological agent of coronavirus disease 19 (COVID-19), which emerged from China in late 2019 and has caused a pandemic.^{1–3} SARS-CoV-2 expresses homotrimeric spike proteins on their surface.^{4,5} The spike monomer comprises two domains (S1 and S2 domains), of which the S1 domain comprises two sub-domains (a receptor-binding domain [RBD] and N-terminal domain [NTD]).⁶

The first step in the infection of human cells involves the SARS-CoV-2 RBD of the spike protein binding to receptor angiotensin-converting enzyme 2 (ACE2) expressed on cells in various tissues, such as lung and the gastrointestinal tract.⁷ Because anti-RBD antibodies that block RBD–ACE2 interaction are capable of inhibiting SARS-CoV-2 infection, major epitopes for SARS-CoV-2-neutralizing antibodies are present in RBD.^{8,9} Recently, many monoclonal antibodies (mAbs) against the RBD of SARS-CoV-2 from convalescent individuals have been generated for COVID-19 therapy, and the casirivimab (REGN10933) and imdevimab

(REGN10987) cocktail therapy and the sotrovimab (VIR-7831) therapy^{10–14} have been approved by the US Food and Drug Administration.

Recent reports of SARS-CoV-2 variants of concerns (VOCs), such as the Alpha (B.1.1.7; N501Y mutation in the RBD), Beta (B.1.351; K417N, E484K, and N501Y mutation in the RBD), Gamma (P.1; K417T, E484K, and N501Y mutation in the RBD), Delta (B.1.617.2; L452R and T478K mutation in the RBD), and Omicron variants (B.1.1.529; G339D, S371L, S373P, S375F, K417N, N440K, G446S, S477N, T478K, E484A, Q493K, G496S, Q498R, N501Y, and Y505H mutation in the RBD),^{15–19} have shown mutations at the antigenic supersite on the ACE2-binding site, which is a major target of potent virus-neutralizing antibodies. Thus, these new variants may impair the efficacy of previously developed monoclonal antibody therapies. Casirivimab and imdevimab cocktail therapy and sotrovimab therapy have been shown to be effective against the Alpha, Beta, Gamma, and Delta variants, but the Omicron variant evaded the protection offered by the majority of SARS-

Tatsuhiko Ozawa  toz@med.u-toyama.ac.jp  Department of Immunology, Faculty of Medicine, Academic Assembly, University of Toyama, 2630 Sugitani, Toyama 930-0194, Japan; CONTACT Hideki Niimi  hiniimi@med.u-toyama.ac.jp  Department of Clinical Laboratory and Molecular Pathology, Faculty of Medicine, Academic Assembly, University of Toyama, 2630 Sugitani, Toyama 930-0194, Japan

[#]These authors contributed equally to this work.

© 2022 The Author(s). Published with license by Taylor & Francis Group, LLC.

This is an Open Access article distributed under the terms of the Creative Commons Attribution-NonCommercial License (<http://creativecommons.org/licenses/by-nc/4.0/>), which permits unrestricted non-commercial use, distribution, and reproduction in any medium, provided the original work is properly cited.

CoV-2 neutralizing antibodies, including casirivimab and imdevimab.^{19–22} At present, only sotrovimab has been suggested to be effective against the Omicron variant, but even so, its neutralization effect was reduced approximately 3-fold.^{11,21,20} Thus, it is urgent that we develop novel antibodies against variants with new mutations, including the Omicron variant. Recently, several SARS-CoV-2 VOC-neutralizing mAbs have been reported.^{23–25}

In this study, we attempted to isolate SARS-CoV-2 VOC-neutralizing mAbs from the peripheral blood lymphocytes of convalescent individuals who recovered from severe COVID-19, as we hypothesized that antibodies with strong neutralization activity would be produced during recovery from a severe condition. As a result, we identified a highly potent neutralizing antibody against SARS-CoV-2 VOCs, UT28K, effective in both *in vitro* and *in vivo* prophylactic treatment. Prophylactic administration of UT28K is expected to confer potent protection against SARS-CoV-2.

Results

Generation of anti-RBD mAbs from peripheral blood B cells of COVID-19 convalescent individuals

First, we screened plasma derived from five COVID-19 convalescent individuals for anti-RBD antibody activities and neutralization activities against SARS-CoV-2. We examined whether or not plasma from these patients was capable of inhibiting the pseudotyped virus infection in VeroE6/TMPRSS2 cells.²⁶ A neutralization assay showed that only the plasma from Pt01 showed neutralization activity against St19pv(G614G) pseudotyped VSV (Supplemental Fig. 1A and B). In addition, plasma from Pt01 showed neutralizing activity against several pseudotyped SARS-CoV-2 VOCs (Alpha, Beta, Gamma, and Delta variants) (Supplemental Fig. 1C and D). We therefore selected Pt01 for the generation of anti-RBD mAbs.

To obtain anti-RBD antibodies from the lymphocytes of Pt01, we used the immunospot array assay on a chip (ISAAC) system^{27,28} and obtained 12 unique anti-RBD mAbs (Supplemental Table 1). We then examined whether or not anti-RBD mAbs were capable of inhibiting spike-ACE2 interaction.

To this end, we performed a competitive enzyme-linked immunosorbent assay (ELISA) in which the spike protein is bound to ACE2 in the presence of anti-RBD mAbs. Five clones (UT28K, UT30L, UT35K, UT55K, and UT61L) clearly inhibited spike-ACE2 (Supplemental Fig. 1E), but UT28K showed the most potent inhibitory activity (Supplemental Fig. 1 F and G). We therefore focused on UT28K for a detailed analysis.

The *in vitro* neutralization activity of UT28K against SARS-CoV-2 mutants

We conducted a detailed investigation of the reactive characteristics of UT28K against SARS-CoV-2 mutants, such as SARS-CoV-2 VOCs (Alpha, Beta, Gamma, Delta, and Omicron) and SARS-CoV-2 formerly monitored variants (Kappa). A neutralization assay using pseudotyped virus demonstrated the neutralization activity of UT28K, with IC₅₀ values against mutants of the pseudotyped virus by UT28K ranging from 40 to 120 pM (Figure 1a), whereas the neutralization activity against the pseudotyped Omicron variant was greatly reduced (Figure 1a, IC₅₀: 200 pM). A yield reduction assay using an authentic virus also showed a reduction in activity against all tested mutants (Figure 1b). While neutralizing activity against the Omicron variant was retained, the neutralization activity of UT28K was reduced by approximately 10-fold in IC₅₀ values compared to wild-type (WT; approximately 500 pM to 5000 pM). These data showed that UT28K was effective against not only WT, but also authentic SARS-CoV-2 mutants tested *in vitro*, whereas its effect was reduced against the Omicron variant.

In vivo protection of UT28K against SARS-CoV-2 mutants

Next, we examined whether or not UT28K was capable of protecting against pseudotyped SARS-CoV-2 infection in a Syrian hamster model as prophylactic treatment.²⁹ To this end, UT28K was intraperitoneally administered to the hamsters. After 24 h, luciferase-expressing pseudotyped SARS-CoV-2 or SARS-CoV-2 mutants were inoculated via intratracheal infection, and another 24 h later, *in vivo* imaging of the lungs showed

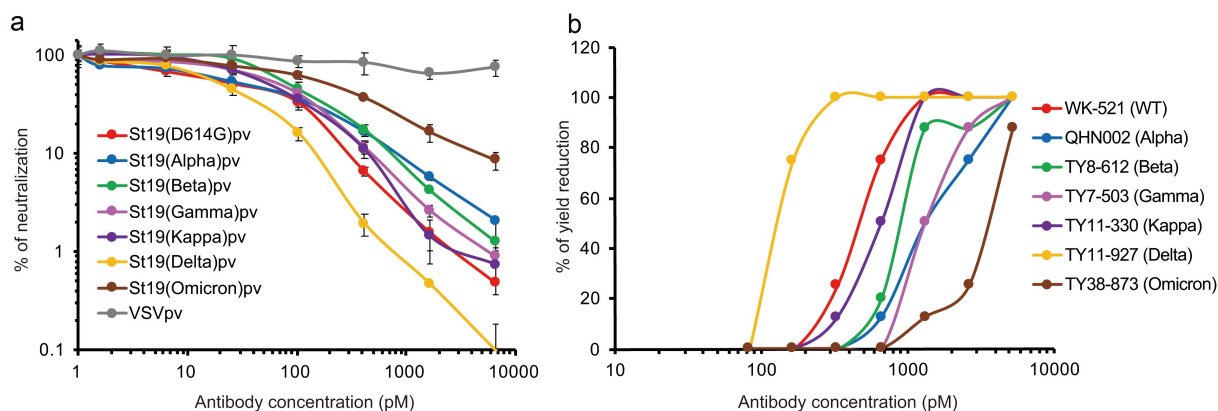


Figure 1. *In vitro* neutralization activity of UT28K mAb. (a, b) Effects on the neutralization of pseudotyped SARS-CoV-2 infections (a) and authentic virus infections (b) through UT28K mAb. The Y-axis indicates the % of neutralization of pseudotyped SARS-CoV-2 infection in VeroE6/TMPRSS2 cells (A) and % of yield reduction (B) in the presence of the indicated concentration of UT28K mAb. Data are shown as the means \pm s.d. of triplicate wells (B). All data are shown a single experiment representative of at least two independent experiments.

that the luminescence had been almost completely reduced in UT28K-treated hamsters (0.3 mg/kg) for Alpha, Gamma, Delta, and Kappa variants (Figure 2a and b). Furthermore, quantitative reverse transcription polymerase chain reaction (RT-qPCR) showed that the viral loads in the lungs were almost eliminated in UT28K-treated hamsters (Figure 2c). In contrast, regarding the Beta and Omicron variants, UT28K was effective at high doses (3 mg/kg, Figure 2b and c), but not at low doses (0.3 mg/kg, data not shown). These results indicate that the prophylactic administration of UT28K to hamsters confers a strong prophylactic effect for protection against tested SARS-CoV-2 mutants, but the effect against the Beta and Omicron variants is weakened. Taken together, our data indicate that intraperitoneal administration of UT28K confers efficacious protection against the tested mutants.

The structure of the UT28K Fab-RBD complex reveals a distinct binding mode

Neutralizing antibodies often utilize public variable region genes, such as IGHV3-53, IGHV3-66, IGHV3-30, IGHV1-2, and IGHV1-69.^{8,30,31} We therefore analyzed the antibody variable gene repertoires. In agreement with previous data,^{8,30,31} our neutralizing antibodies (UT30L, UT55K, and UT61L) utilize public V_H genes (Supplemental Table 1). However, instead

of these stereotypic V_H genes, UT28K utilized the IGHV1-58/IGKV3-20 pair (Supplemental Table 1). IGHV1-58/IGKV3-20 paired antibodies have been reported to not only bind to the SARS-CoV-2 RBD avidly, but also to neutralize viruses with high potency and include COV2-2196,³² S2E12,³³ 253H53L,³⁴ A23-58.1, and B1-182.1.³⁵ The sequences of UT28K were very similar to those of previously reported mAbs (Supplemental Fig. 2). Structural analysis of the IGHV1-58/IGKV3-20 paired mAb in complex with the RBD revealed how the IGHV1-58/IGKV3-20 paired mAb recognizes the RBD.³²⁻³⁵

To gain structural insight into the interaction of UT28K antibody with the SARS-CoV-2 spike (S) protein, we performed a cryo-electron microscopy (EM) analysis of the SARS-CoV-2 S protein ectodomain bound to Fab UT28K and determined the cryo-EM map with C3 symmetry at a resolution of 3.1 Å. Fab UT28K recognized the left shoulder of the RBD in the up form (EMDB ID: EMD-33045, (Figure 3a), Supplemental Fig. 3, Supplemental Table 2), and the binding mode of Fab UT28K was almost the same as in previously reported IGHV1-58/IGKV3-20 pairing mAbs, such as COV2-2196,³² S2E12,³³ 253H53L,³⁴ A23-58.1, and B1-182.1.³⁵ In the cryo-EM map, the local resolution of Fab UT28K and the RBD was low at approximately 5 Å. Therefore, we further performed X-ray crystallography of the CoV-2 S protein RBD in complex with Fab UT28K.

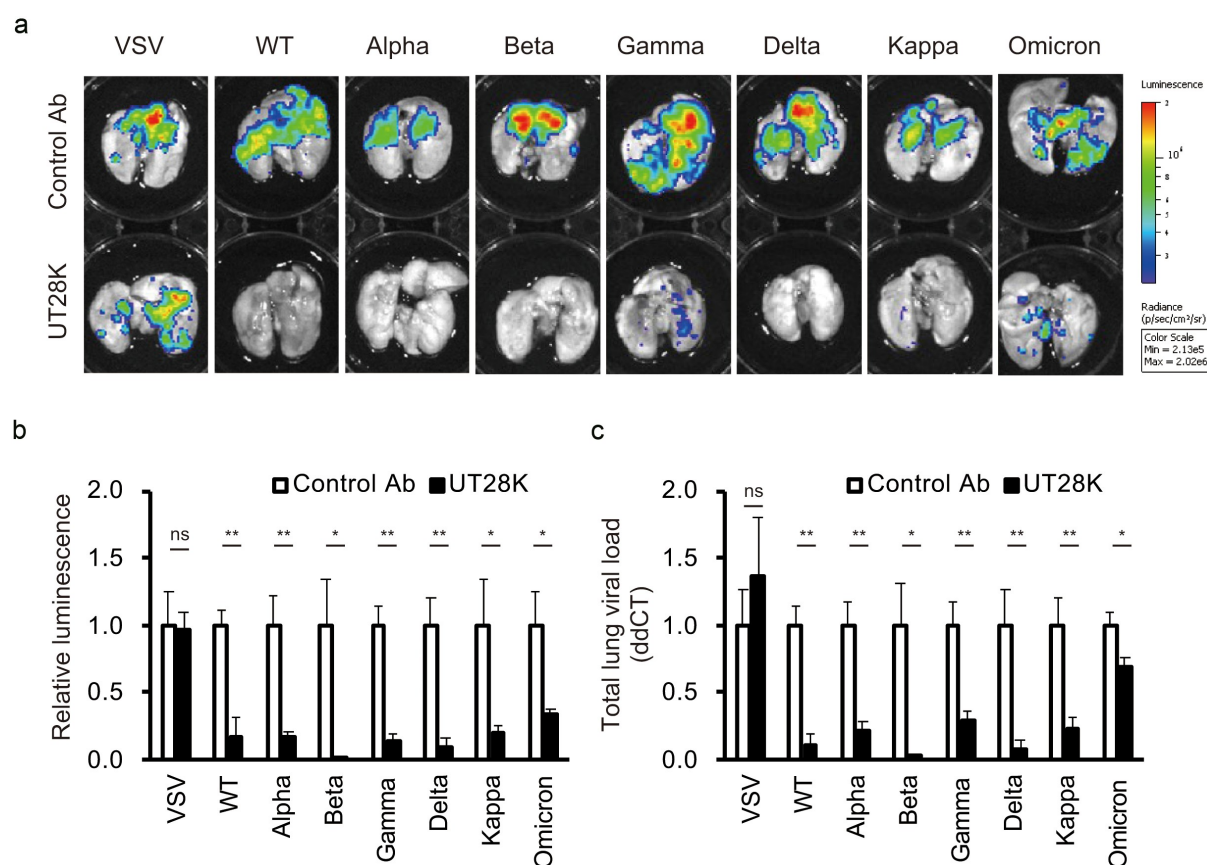


Figure 2. Pseudotyped SARS-CoV-2 infection in hamster model at prophylactic treatment. (a) Representative IVIS images of the lungs of individual hamsters are shown. (b) The luminescence measurements from the lungs infected by luciferase-expressing pseudotyped SARS-CoV-2. The Y-axis indicates the relative luminescence level to control antibody. (c) RT-qPCR was used to measure the VSV N expression in lung tissues. Data are shown as the means \pm s.d. *p*-values were calculated using Student's *t*-test (*, *p* < .05 and **, *p* < .01).

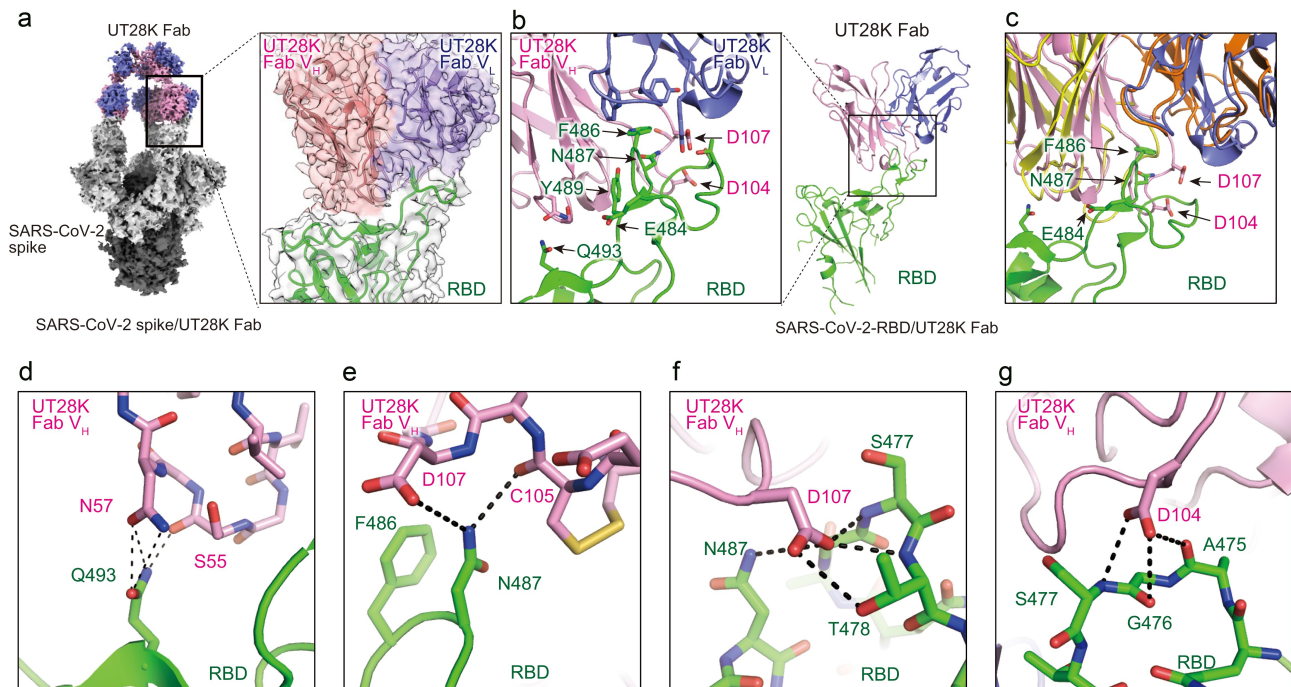


Figure 3. Structures of antibody UT28K bound to the SARS-CoV-2 S protein and their interactions. (a) Cryo-EM structure of Fab UT28K bound to the SARS-CoV-2 S protein trimer. The heavy and light chains of Fab UT28K are shown in pink and marine blue, respectively. The S1 and S2 subunits are shown in gray and black, respectively. The N-linked glycans are shown in cyan. (b) The crystal structure of Fab UT28K bound to the SARS-CoV-2 S protein RBD. The colors of Fab UT28K are the same as shown in A. The SARS-CoV-2 S RBD is shown in green. (c) A comparison of the binding modes of antibodies UT28K and 253XL55 (V_H; yellow and V_L; Orange) bound to the SARS-CoV-2 S protein RBD. (d-g) Interactions of key residues between Fab UT28K and the SARS-CoV-2 S RBD.

By determining the X-ray crystal structure at the resolution of 3.75 Å, we confirmed that Fab UT28K recognizes the same region as the cryo-EM structure (PDB ID: 7X70, Figure 3b, Supplemental Table 3). The antibody UT28K recognized F486 of the RBD as a core interacting amino acid residue and interacted with the hydrophobic pocket of the antibody. This binding mode was similar to that in antibodies with closely related sequences, such as S2E12 (PDB ID; 7R6X), 253XL55 (PDB ID; 7BEO), and COV-2196 (PDB ID; 7L7D) (Figure 3c). Aside from these interactions, the side chain of RBD Q493 formed hydrogen bonds with V_H S55 and N57 of Fab UT28K (Figure 3d).

As unique interactions for Fab UT28K that depend on amino acid sequences different from the closely related antibodies described above, the side chain of RBD N487 formed hydrogen bonds with the side chain of V_H D107 of Fab UT28K and with the oxygen atoms of the main chains of V_H C105 and V_H S106 of Fab UT28K (Figure 3e). The side chain of V_H D107 of Fab UT28K formed hydrogen bonds with the side chains and nitrogen atoms of the main chains of S477 and T478, in addition to the RBD N487 (figure 3f). Furthermore, the side chain of V_H D104 of Fab UT28K formed hydrogen bonds with the nitrogen atoms of the main chain of RBD S477 and with the oxygen atoms of the main chains of A475 and G476 (Figure 3g). N487 of the RBD and V_H D104 and V_H D107 of antibody UT28K, key residues for antigen-antibody interaction, thus recognize the main chains of the interacting molecules, resulting in unique interaction.

Epitope mapping of UT28K mAb

To investigate whether or not UT28K recognizes F486, we performed epitope mapping. To this end, we examined the ability of each mutant RBD protein to bind to UT28K using an ELISA. UT28K did not react with F486S or N487R of mutant RBD proteins, but showed no significant reduction in binding to other tested mutant RBD proteins (Figure 4a). These results show that at least F486 and N487 of the RBD protein are indispensable for the binding of UT28K, similar to previously reported IGHV1-58/IGKV3-20 paired antibodies.^{14,32-35}

Next, we investigated which mutations have the potential to arise during viral growth under UT28K, and it was found that the Y489H mutation was contained in the S region in all three prototype strains that were independently tested (Figure 4b). In contrast, this mutation was not observed in the viral growth under the culture condition with the control antibody that recognizes the West Nile virus envelope protein.

Discussion

Recent reports for SARS-CoV-2 and other virus-neutralizing mAbs have described the identification of public mAbs, i.e., similar antibodies isolated from multiple individuals.^{30,32,36-38} Among public SARS-CoV-2 mAbs, several potent neutralization mAbs that utilize the IGHV1-58/IGKV3-20 pair have been reported.^{14,30,33-35,39-41} The key epitopes of this public mAbs were shown to include at least F486 on the RBD.^{14,32-35} Our

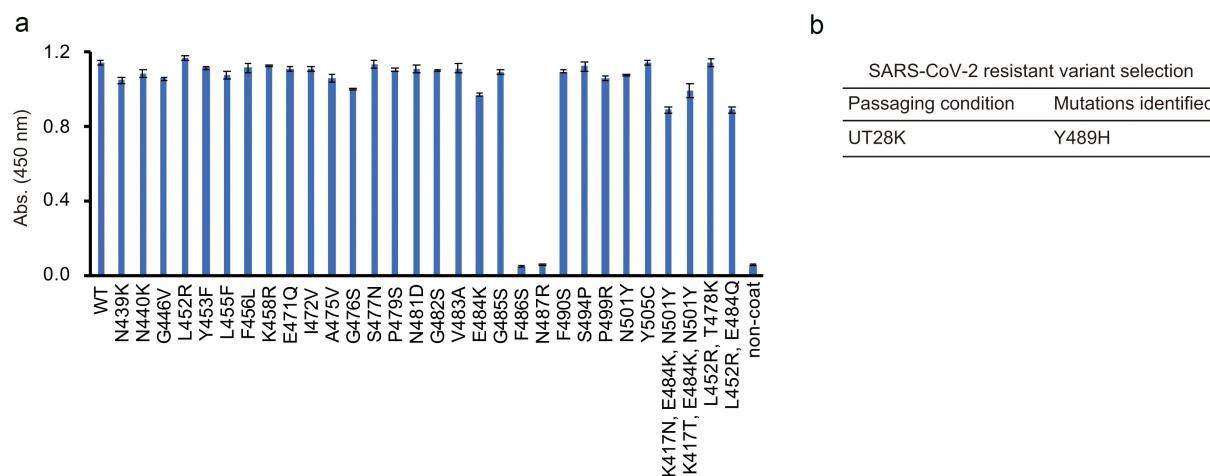


Figure 4. Epitope mapping of UT28K mAb. (a) The binding capacity of UT28K to individual mutant RBD proteins was examined by an ELISA. Data are shown as the means \pm s.d. of triplicate wells. Data are representative of at least two independent experiments that were performed with similar results. (b) Table showing the results of the passage SARS-CoV-2 escape selection experiments.

UT28K also utilizes the IGHV1-58/IGKV3-20 pair (Supplemental Table 1) and shows very similar amino acid sequences of complementarity-determining regions (CDRs) to previously reported mAbs (Supplemental Fig. 2). The key epitopes of UT28K were F486 and N487 on the RBD (Figure 3). Thus, UT28K is suggested also to be a public mAb that utilizes the IGHV1-58/IGKV3-20 pair.

Although UT28K is also a public mAb that utilizes the IGHV1-58/IGKV3-20 pair and the sequences of UT28K are very similar to those of previously reported mAbs, the binding modes of the antibody UT28K Fab and SARS-CoV-2 RBD protein show unique interactions with the main chain in the epitope (Figure 3). The structure of public mAb that utilizes the IGHV1-58/IGKV3-20 pair has been analyzed, but the binding to the main chain is not mentioned in detail so far. As an appropriate example of its interactions with the main chains, no structural data was available for other strongly neutralizing antibodies against SARS-CoV2. Therefore, example of antibody 10A37 that neutralized HIV-1^{42,43} was used for comparison here. In their study of the interaction with the main chain in the epitope, Pan et al. showed that 10A37, a neutralization antibody against different clades of HIV-1 with high potency, is a main chain-dominated antigen-antibody interaction, and this interaction explained the broad neutralization of 10A37.^{42,43} UT28K is similar to 10A37, and there are at least four main-chain interactions (A475, G476, S477, and T478) and at least three side-chain interactions (F486, N487, Q493) between the RBD and UT28K (Figure 3). These interactions also reflect the reactivity in epitope mapping. The epitope mapping analysis showed that UT28K reacted with A475V, G476S, S477N, and T478K, which interacted with the main chain, but did not react with many mutations F486S and N487R, which interacted with the side chain (Figure 4a). Because the mutant RBD for Q493 was not available, it could not be examined. These amino acid substitutions in the RBD are

located at the center of the antigen-antibody binding site and are consistent with the structural information. Therefore, these data indicate that UT28K is a main chain-dominated antigen-antibody interaction. The shorter HCDR3 loop of UT28K compared to closely related antibodies, such as S2E12, 253XL55, and COV-2196, may support the recognition of the main chains of the RBD by D104 in UT28K. The N487 and Y489 (Figure 4b) of the RBD may support the orientation of the F486 of the RBD for interacting with the hydrophobic pocket of UT28K, as amino-acid substitutions in N487 and Y489 of the RBD cause it to evade antibody recognition.

In addition, the amino acid residue E484 of RBD, which plays an important role in decreasing the reactivity of neutralizing antibodies in VOCs, is located outside of the antibody binding site (Figure 3c), indicating that antibody UT28K is structurally independent of the E484 amino acid substitution. This feature, along with the unique interaction recognizing a wide range of main-chain atoms of the RBD, may be the structural basis for the high neutralizing ability of UT28K. However, the response to the Omicron variant was reduced (Figures 1 and 2). We considered this to be due to the Q493R mutation, one of the mutations of the Omicron variant, causing the obliteration of hydrogen bonds or a steric hindrance to RBD binding (Figure 3d).

When mutations occur at the F486, N487, and Y489 residues, these mutant viruses can evade UT28K. (Figure 4a,b). However, a recent analysis showed that F486 and N487 are important residues for interaction with ACE2, suggesting that these mutations may reduce or abolish the infectivity of SARS-CoV-2.⁴⁴⁻⁴⁷ In addition, the frequency of these substitutions among viruses in the GISAID databases thus far is exceedingly rare (all $\leq 0.001\%$ when investigated on March 10, 2022). Thus, F486, N487, and Y489 mutations likely lose their competitive advantage over circulating SARS-CoV-2. As such, the emergence of a UT28K neutralization-resistant SARS-CoV-2 variant is unlikely.

UT28K contains non-canonical cysteine motif, CX₃C⁴⁸ and formed intra-CDR-H3 disulfide bonds (Figure 3e). It has been reported that CDR-H3s with this motif were found to adopt β -hairpin folds as stabilized by disulfide bridges, and CDR-H3 motifs in human antibodies play important roles in antigen recognition.⁴⁸ Investigating the relationship between this motif and the broad and potent neutralizing activity of UT28K may lead to a therapeutic antibody useful for COVID-19.

In summary, we identified a potent SARS-CoV-2 mutant-neutralizing antibody, UT28K, in a COVID-19 convalescent individual. An *in vitro* assay and prophylactic administration assay showed that UT28K could protect against the tested SARS-CoV-2 mutants, but had reduced neutralization activity against the Omicron variant. An X-ray crystallography analysis revealed that UT28K is a main chain-dominated antigen-antibody interaction, and this interaction explained the broad neutralization against SARS-CoV-2 mutants. Furthermore, an epitope mapping analysis suggested that the emergence of a UT28K neutralization-resistant SARS-CoV-2 variant was unlikely, as such a variant was likely to lose its competitive advantage over circulating SARS-CoV-2. Because UT28K cDNA is encoded by the IGHV1-58/IGKV3-20 pair, and its epitopes are F486 and N487 on the SARS-CoV-2 S protein, UT28K is suggested to be a public mAb that utilizes the IGHV1-58/IGKV3-20 pair. These data suggest that UT28K is a viable new SARS-CoV-2 mutant-neutralizing mAb. UT28K will likely confer potent protection against SARS-CoV-2 mutants, including new emerging variants, along with vaccines.

Materials and methods

Patients

All procedures were performed under a protocol approved by the Ethics Committee of the University of Toyama (approval No. R2020152), and written informed consent was obtained from all patients. The methods were carried out in accordance with the approved guidelines.

Five adult COVID-19 patients with different disease severities who visited or were admitted to Toyama University Hospital from September 28 to December 28, 2020, were included in this study. They were diagnosed with COVID-19 based on a positive nasopharyngeal SARS-CoV-2 RT-PCR result. Chest computed tomography was performed in all patients, and the severity was divided into five categories: asymptomatic, mild (symptomatic patients without pneumonia), moderate (pneumonia patients without required oxygen supplementation), severe (required oxygen supplementation), and critically ill (requiring invasive mechanical ventilation, shock, and/or multiple organ dysfunction). Of the five patients enrolled in this study, two were asymptomatic (Pt03 and Pt04), and the rest had fully recovered from a moderate (Pt02) or critically ill condition (Pt01 and Pt05). Whole blood to obtain peripheral blood lymphocytes was collected at 9–13, 9, and 33–34 days after the diagnosis or onset in the asymptomatic, moderate, and critically ill patients, respectively.

Viruses

The SARS-CoV-2 virus prototype, hCoV-19/Japan/TY/WK-521/2020 (A, GSAID ID: EPI_ISL_408667), and the Alpha variant; hCoV-19/Japan/QHN002/2020 (B.1.1.7, GSAID ID: EPI_ISL_804008), Beta variant; hCoV-19/Japan/TY8-612/2021 (B.1.351, GSAID ID: EPI_ISL_1123289), Gamma variant; hCoV-19/Japan/TY7-503/2021 (P.1, GSAID ID: EPI_ISL_833369), Kappa variant; hCoV-19/Japan/TY11-330/2021 (B.1.617.1, GSAID ID: EPI_ISL_2158613), Delta variant; hCoV-19/Japan/TY11-927/2021 (B.1.617.2, GSAID ID: EPI_ISL_2158617), and Omicron variant; hCoV-19/Japan/TY38-873 (B.1.1.529, GSAID ID: EPI_ISL_7418017), which were isolated at the National Institute of Infectious Diseases in Japan, were kindly provided by the National Institute of Infectious Diseases in Japan.

Pseudotyped VSV bearing the SARS-CoV-2 S protein was generated as previously described.²⁶ The expression plasmids for the truncated mutant S protein of SARS-CoV-2, pCAGG-pm3-SARS2-Shu-d19_D614G (Prototype), pCAGG-pm3-SARS2-Shu-d19-B.1.1.7 (Alpha variant), pCAGG-pm3-SARS2-Shu-d19-B.1.351 (Beta variant), pCAGG-pm3-SARS2-Shu-d19-P.1 (Gamma variant), pCAGG-pm3-SARS2-Shu-d19-B.1.617.1 (Kappa variant), pCAGG-pm3-SARS2-Shu-d19-B.1.617.2 (Delta variant), and pCAGG-pm3-SARS2-SHu-d19-BA.1_EPE_3mut_Omi (Omicron variant) were constructed as described previously.⁴⁹ In brief, 293 T cells on collagen-coated tissue culture plates were transfected with the above expression vectors. After 24 h of incubation, the transfected cells were infected with G-complemented (*G) VSV Δ G/Luc (*G-VSV Δ G/Luc)⁵⁰ at a multiplicity of infection of 0.5. The virus was adsorbed and extensively washed 4 times with Dulbecco's modified Eagle's medium (DMEM) supplemented with 10% fetal bovine serum (FBS). After another 24 h of incubation, the culture supernatants containing pseudotyped VSVs were centrifuged to remove cell debris and stored at -80°C until further use.

Detection of ASCs using ISAAC and isolation of antibody cDNA and the production and purification of antibodies

Peripheral blood mononuclear cells (PBMCs) were prepared from 40 ml of heparinized blood from each patient by centrifugation at $400 \times g$ on a Ficoll-Hypaque density-gradient and stored in -80°C with CellBankerTM 1 (Nippon Zenyaku Kogyo, Fukushima, Japan) cryopreservative medium until use. After thawing, PBMCs were cultured as described previously.⁵¹ We then isolated CD138⁺ cells using human CD138 MicroBeads (Miltenyi Biotec, Bergisch Gladbach, Germany) and MS columns (Miltenyi Biotec) as described by the manufacturer.

The ISAAC method is covered by patents that have been exclusively licensed to Valneva (Nantes, France). Details and instructions regarding the microwell array chip and the ISAAC method have been previously described.^{27,28} In brief, we coated the surface of the chip with 10 $\mu\text{g/ml}$ SARS-CoV-2 spike protein (ACRO Biosystems, Newark, DE) or SARS-CoV-2 RBD protein (Sino Biological, Wayne, PA) in phosphate-buffered saline (PBS) and incubated it overnight at 4°C . After removing the antigen solution, we blocked the chip with 0.01% Biolipidure (NOF Corporation, Tokyo, Japan) for 30 min at room temperature and subsequently washed it with the culture medium. We then arrayed

the CD138⁺ cells in culture medium to the chip and removed residual cells outside the wells with gentle washing. We cultured the cells on the chip for 3 h at 37°C. After gentle washing, we added 10 µg/ml Cy3-conjugated anti-human IgG Fc (Merck Millipore, Burlington, MA) and performed incubation for 30 min. Finally, we stained the cells with 1 µM Oregon Green (Thermo Fisher Scientific, Waltham, MA) for 5 min at room temperature. Antigen-specific antibodies released from single cells were observed under a fluorescence microscope (BX51WI; Olympus, Tokyo, Japan).

Details regarding the amplification of antibody cDNA from single cells and the construction of the pcDNA3.4 expression vector (Thermo Fisher Scientific, Waltham, MA, USA) were described previously.^{27,28} Afterward, we cotransfected Expi293FTM cells with both the heavy and light chain expression vectors encoding the entire antibody molecules using the Expi293TM Expression System (Thermo Fisher Scientific). We then collected the supernatant from cultured cells and purified the antibody using a protein G column (Cytiva, Tokyo, Japan), as previously described.^{28,52,53} The immunoglobulin gene repertoire was analyzed with the IMG2/V-Quest tool⁵⁴ (<http://www.imgt.org/>). The control monoclonal antibody was WN_11, which recognizes the West Nile virus envelope protein.⁵³

ELISA

To analyze the antibody binding to spike and RBD protein, we coated the wells of 96-well MaxiSorp plates (Thermo Fisher Scientific) with 50 µl of 1 µg/ml protein in PBS and subsequently blocked nonspecific protein binding with 3% bovine serum albumin (BSA) in PBS. After washing, we added antibodies to the plates and incubated them at room temperature (RT) for 1 h. After washing, we detected the antibodies that had bound to protein using horseradish peroxidase-conjugated anti-human IgG-Fc specific antibodies (Cat. No: SAB3701270; Sigma-Aldrich, St Louis, MO) and 3,3',5,5'-tetramethylbenzidine (TMB) substrate (SeraCare Life Sciences, Milford, MA). Optical absorbance at 450 nm was measured using the OPTIMA plate reader (BMG LABTECH, Ortenberg, Germany).

To analyze the inhibition of spike or RBD protein-ACE2 interaction by antibodies, we coated the wells of 96-well MaxiSorp plates with 50 µl of 1 µg/ml RBD protein in PBS and subsequently blocked nonspecific protein binding with 3% BSA in PBS. After washing, we added 50 ng/ml biotinylated ACE2 along with antibody (10 µg/ml to 20 ng/ml) or not antibody to the plates for incubation at RT for 1 h. After washing, we detected the ACE2 that had bound to RBD protein using horseradish peroxidase-conjugated streptavidins (Abcam, Cambridge, UK) and TMB substrate. Optical absorbance at 450 nm was measured using the OPTIMA plate reader.

A neutralization assay using pseudotyped viruses

The patient sera used in this study were collected from participants after obtaining their informed consent. To examine the neutralization of the human serum specimens or mAbs against pseudotyped viruses, VeroE6/TMPRSS2 cells purchased from

the Japanese Collection of Research Bioresources (JCRB) Cell Bank (the National Institute of Biomedical Innovation, Health, and Nutrition, Osaka, Japan) (JCRB1819) were treated with serially diluted sera of convalescent patients with COVID-19 or mAbs and then inoculated with St19pv(D614G), St19pv(alpha), St19pv(beta), St19pv(gamma), St19pv(kappa), St19pv(delta), St19pv(omicron), or VSVpv. The infectivities of the pseudotyped viruses were determined by measuring the luciferase activities using a PicaGene Luminescence Kit (Fujifilm Wako, Osaka, Japan) with a GloMax Navigator Microplate Luminometer (Promega, Madison, WI) after 24 h of incubation at 37°C. The IC₅₀ was calculated by Prism 7 and represented as the neutralization titer.

A neutralization assay using authentic viruses

The neutralizing activity of mAbs against authentic SARS-CoV-2 was determined by a neutralization test in a biosafety level 3 laboratory of Toyama Institute of Health. For the 96-well neutralization assay, VeroE6/TMPRSS2 cells were plated at 2×10^4 cells per well and infected with the indicated strains of SARS-CoV-2 at a multiplicity of infection (MOI) of 0.001 per cell in the presence of serially 2-fold diluted mAbs. After 1-h incubation, culture supernatants were discarded and cultured for 24 h with DMEM containing 10% FBS in the presence of the indicated concentration of mAbs. Supernatants were then collected from the cell cultures. The viral infectious dose of each supernatant was determined by a quantity of viral genomic RNA using a real-time PCR assay with a SARS-CoV-2 direct detection RT-qPCR kit (Takara Bio Inc., Siga, Japan). The IC₅₀ was calculated by Prism 7 and represented as the neutralization titer.

The *in vivo* prophylactic treatment assay

The Ethics Review Committee for Animal Experimentation approved all experimental protocols used in this study (Protocol Number: A2020MED-18).

Male 6- to 10-week-old hamsters were purchased from Japan SLC Inc. (Shizuoka, Japan). All animals were housed in a pathogen-free environment at the Division of Animal Resources and Development at the University of Toyama. Antibody (0.3 or 3 mg per hamster) was administered intraperitoneally to the hamsters. After 24 h, virus solution was directly inoculated into the trachea, as previously described.²⁹ The hamsters were sacrificed by isoflurane and cervical dislocation 24 h after infection. The lungs were harvested and incubated with 1 mg/mL of D-luciferin (Promega) for 5 min. Luminescence was measured using an *in vivo* imaging system (IVIS Lumina II; Perkin Elmer, MA, USA). Analyses were performed using the Living Image 4.2 software program (Caliper Life Science, Waltham, MA) to measure the light emitting from the infection sites. The luminescence from the front and back of the lungs was measured, and the sum was calculated.

To evaluate viral infection, the VSV N gene expression in the lungs was measured using a quantitative polymerase chain reaction.²⁹ In brief, after homogenizing the lungs using a BeadMill 24 (Thermo Fisher Scientific), homogenized lung solution was immediately mixed with Isogen (Nippon Gene, Toyama, Japan) and stored at -80°C. The total RNA was extracted using a QIAamp Viral RNA Mini Kit (Qiagen, Hilden, Germany)

according to the manufacturer's instructions. The total RNA was reverse transcribed into cDNA and then amplified using a Thunderbird SYBR qPCR/RT Set III (TOYOBO, Tsuruga, Japan). The VSV N expression was normalized to that of γ -actin.

Expression and purification of recombinant UT28K Fab

To generate UT28K Fab, we inserted the DNA fragment of the UT28K V_H gene into expression vectors consisting of the following elements starting from the N terminus: a constant region of human IgG CH₁, flexible linker GSSG, and a decahistidine His₁₀ tag. We then co-transfected Expi293 FTM cells with both the Fab and light chain expression vectors encoding the Fab molecules using the Expi293TM Expression System. Next, we collected the supernatant from cultured cells and dialyzed it using the dialysis membrane (Spectrum Laboratories, Rancho Dominguez, CA, USA). The membrane was soaked in native buffer (20 mM sodium phosphate, 0.5 M NaCl, pH 7.4) in a container with a cover and shaken in a shaker at 4°C for up to 72 h. The proteins were then purified by affinity chromatography using Ni Sepharose 6 Fast Flow (Cytiva) according to the manufacturer's instructions. A Poly-Prep column (Bio-Rad, Hercules, CA, USA) packed with Ni Sepharose 6 Fast Flow mix was loaded with pretreated supernatant, washed with native buffer containing 20 mM imidazole, and then washed with native buffer containing 50 mM imidazole. Finally, Fab molecules were eluted with Elution Buffer (20 mM sodium phosphate, 0.5 M NaCl, 500 mM imidazole, pH 7.4). The concentrations of purified Fab were measured using a NanoDrop 2000 (Thermo Fisher Scientific).

Crystallization, data collection, and structural determination

The protein of SARS-CoV-2 spike RBD was expressed and purified by the same procedure as previously reported.²³ Purified SARS-CoV-2 RBD and UT28K Fabs were mixed at a molar ratio of 1:1.3, and then the RBD-Fab complex was purified by a superdex200 10/300 (Cytiva) equilibrated with 20 mM Tris pH 8.0 and 100 mM NaCl. The fraction containing both the RBD and Fab were collected and concentrated to 13 mg/ml. Crystallization screening was performed by a crystallization robot mosquito using commercially available screening kits. Crystals of RBD-Fab complex were grown at 293 K by the sitting drop vapor-diffusion method. The final crystallization condition was 0.1 M citric acid pH 5.0, 1.0 M lithium chloride, 10% (w/v) PEG 6000.

The crystals were cryo-cooled in liquid nitrogen, and an X-ray diffraction experiment was performed at beamline BL32XU of SPring-8 (Harima, Japan). The X-ray diffraction data set was processed with XDS and scaled with Aimless in the CCP4 program package.^{55–57} The structure was solved by the molecular replacement method using the Phaser program in the PHENIX package. The RBD structure (PDB ID: 7jmb), and the UT28K Fabs generated with the alphafold2 colab website were used as search probes for molecular replacement. The structure refinement was carried out using phenix.refine and COOT.^{58,59} The stereochemical properties of the structure were assessed using MolProbity.⁶⁰ Figures were prepared with

PyMOL (<http://pymol.sourceforge.net>). Intermolecular contact atoms were analyzed using PISA and CONTACT in the CCP4 program package.⁶¹

Cryo-EM sample preparation and data collection

To prepare a complex sample for cryo-EM, SARS-CoV-2 spike 6P solution was incubated at 37°C for 1 hour before use. The protein of SARS-CoV-2 spike 6P was expressed and purified by the same procedure as previously reported.²³ The purified UT28K Fabs were incubated with SARS-CoV-2 spike 6P at a molar ratio of 1:2 at 18°C for 1 h. The sample was then applied to a Quantifoil R1.2/1.3 Cu 300 mesh grid (Quantifoil Micro Tools GmbH, Jena, Germany), which had been freshly glow-discharged for 120 s at 10 mA using PIB-10 (Vacuum Device, Mito, Japan). The sample was plunged into liquid ethane using a Vitrobot mark IV (Thermo Fisher Scientific) with the following settings: temperature 18°C, humidity 100%, blotting time 5 s, and blotting force 5.

Micrographs were collected on a Krios G4 (Thermo Fisher Scientific) operated at 300 kV with a K3 direct electron detector (Gatan, Pleasanton, CA) at a nominal magnification of 130,000 (0.67 per physical pixel), using a GIF-Biocontinuum energy filter (Gatan) with a 20-eV slit width. Each micrograph was collected with a total exposure of 1.5 s and a total dose of 53.14 e/Å² over 50 frames. A total of 2217 micrographs were collected at a nominal defocus range of 1.0–2.0 μ m using EPU software (Thermo Fisher Scientific).

Cryo-EM image processing

All image processing steps were performed in Relion 3.1.^{62,63} Micrograph movie frames were aligned and dose-weighted using MotionCor2.⁶⁴ The contrast transfer function estimation was performed with CTFFIND4,⁶⁵ and 2073 micrographs were selected. A total of 711242 particles were auto-picked based on the template generated by particle picking using the Laplacian-Gaussian filter and several rounds of two-dimensional (2D) classification. Next, three-dimensional (3D) classification and 2D classification were performed to remove junk particles. One further round of 3D classification was then performed to identify one class containing one spike with three Fabs. This class included 56,247 particles used in the final 3D reconstruction with C3 symmetry to generate a map with a resolution of 3.1 Å after CTF refinement and Bayesian polishing. The reported resolutions are based on the gold-standard Fourier shell correlation curves (FSC = 0.143) criterion. Local resolution was estimated using RELION implemented local resolution estimation. Figures were prepared with Chimera and Chimera X.⁶⁶

Selection of mAb-escape mutants of SARS-CoV-2

Prototype (Wuhan strain) of authentic SARS-CoV-2 was pre-incubated with a 90% inhibitory concentration (IC₉₀) of UT28K or control mAb (WN_11) that recognizes the West Nile virus envelope protein (1.0 μ g/ml) and inoculated into VeroE6/TMPRSS2 cells. Culture supernatants were harvested at 72 h post infection and passaged again by doubling the amount of mAb for subsequent passage. After three passages, culture supernatants were harvested. The viral RNA was

isolated using a QIAamp Viral RNA Mini Kit (Qiagen) according to the manufacturer's instructions. Whole-genome amplification of escape mutants was carried out using a modified version of the ARTIC Network's protocol for SARS-CoV-2 genome sequencing.⁶⁷ A next-generation sequencing (NGS) library was constructed using the QIAseq FX DNA Library kit (Qiagen) and sequenced using the iSeq platform (Illumina, San Diego, CA). NGS reads were mapped to the SARS-CoV-2 Wuhan-Hu-1 reference genome sequence (GenBank accession no. MN908947.3) using the bwa mem algorithm (version 0.7.13-r1126);⁶⁸ next, a variant allele frequency analysis was conducted using VarScan version 2.4.3.^{69,70}

Acknowledgments

We thank Sanae Hirota, Sakurako Ushijima, Yoshihiro Yoshida, and Mina Sasaki for technical assistance, and Kaoru Hata for secretarial work. The S protein expression plasmids were kindly provided by Chikako Ono and Yoshiharu Matsuura (Research Institute for Microbial Diseases, Osaka University).

Author contributions

T.O., H.T., Y.M., Sh.S., N.H., and I.K. designed the study. T.O., H.T., S.K., E.L., Y.S., N.L., Y.A., H.Ka., H.Y., S.Sas., M.S., J.S., T.H., and H.F. performed the experiments. T.O., H.K., S.K., Y.A., Y.H., Y.Y., Y.M., N.K., M.I., T.H., H.F., K.M., H.Ki., H.N., and U.K. performed analysis and interpretation of data. H.Ka. and Y.Y. collected clinical samples. T.O., H.T., S.K., Y.A., Y.Y., Y.M., T.H., K.M., H.Ki., and H.N. wrote and edited the manuscript.

Abbreviations

ACE2, angiotensin-converting enzyme 2; CDR, complementarity-determining region; COVID-19, coronavirus disease 19; cryo-EM, cryo-electron microscopy; ISAAC, immunospot array assay on a chip; mAb, monoclonal antibody; RBD, receptor-binding domain; SARS-CoV-2, severe acute respiratory syndrome coronavirus 2; VOC, variants of concern

Disclosure statement

No potential conflict of interest was reported by the author(s).

Funding

This work was supported by Discretionary Fund of the President of the University of Toyama (H.N.), Grant for the Promotion of National University Reform from the Ministry of Education, Culture, Sports, Science and Technology (H.N.), Grant from the Toyama Pharmaceutical Valley Development Consortium (H.N.), the Platform Project for Supporting Drug Discovery and Life Science Research (Basis for Supporting Innovative Drug Discovery and Life Science Research (BINDS)) from AMED under grant number JP21am0101077 (T.O.), and JP21am0101093 (K.M.), Ministry of Education, Culture, Sports, Science and Technology grant 20H05773 (T.H.) and JST CREST Grant Number JPMJCR20H8 (T.H.), the Takeda Foundation (K.M.) and Joint Usage/Research Center program of Institute for Frontier Life and Medical Sciences, Kyoto University (K.M.).

ORCID

Tatsuhiko Ozawa  <http://orcid.org/0000-0002-3112-452X>
 Hideki Tani  <http://orcid.org/0000-0002-6309-277X>
 Yuki Anraku  <http://orcid.org/0000-0002-5731-0902>
 Shunsuke Kita  <http://orcid.org/0000-0003-3969-302X>
 Hiroshi Yamada  <http://orcid.org/0000-0001-6678-2701>
 Mayu Somekawa  <http://orcid.org/0000-0002-5923-2530>
 Yoshihiro Hayakawa  <http://orcid.org/0000-0002-7921-1171>
 Yoshihiro Yamamoto  <http://orcid.org/0000-0003-2088-8724>
 Yoshitomo Morinaga  <http://orcid.org/0000-0002-3827-6411>
 Nobuyuki Kurosawa  <http://orcid.org/0000-0002-1548-4541>
 Masaharu Isobe  <http://orcid.org/0000-0003-1864-9273>
 Hideo Fukuhara  <http://orcid.org/0000-0002-7035-8206>
 Katsumi Maenaka  <http://orcid.org/0000-0002-5459-521X>
 Takao Hashiguchi  <http://orcid.org/0000-0001-7578-7571>
 Hiroyuki Kishi  <http://orcid.org/0000-0002-8740-5371>
 Isao Kitajima  <http://orcid.org/0000-0001-6156-4481>
 Shigeru Saito  <http://orcid.org/0000-0002-8940-3708>
 Hideki Niimi  <http://orcid.org/0000-0002-6838-5846>

References

- Li Q, Guan X, Wu P, Wang X, Zhou L, Tong Y, Ren R, Leung KSM, Lau EHY, Wong JY, et al. Early transmission dynamics in Wuhan, China, of novel coronavirus-infected pneumonia. *The New England Journal of Medicine*. 2020;382(13):1199–207. doi:10.1056/NEJMoa2001316.
- Huang C, Wang Y, Li X, Ren L, Zhao J, Hu Y, Zhang L, Fan G, Xu J, Gu X, et al. Clinical features of patients infected with 2019 novel coronavirus in Wuhan, China. *Lancet*. 2020;395(10223):497–506. doi:10.1016/S0140-6736(20)30183-5.
- Wang D, Hu B, Hu C, Zhu F, Liu X, Zhang J, Wang B, Xiang H, Cheng Z, Xiong Y, et al. Clinical characteristics of 138 hospitalized patients with 2019 novel coronavirus–infected pneumonia in Wuhan, China. *JAMA*. 2020;323(11):1061–69. doi:10.1001/jama.2020.1585.
- Yao H, Song Y, Chen Y, Wu N, Xu J, Sun C, Zhang J, Weng T, Zhang Z, Wu Z, et al. Molecular architecture of the SARS-CoV-2 virus. *Cell*. 2020;183(3):730–8 e13. doi:10.1016/j.cell.2020.09.018.
- Turonova B, Sikora M, Schurmann C, Hagen WJH, Welsch S, Blanc FEC, von Bulow S, Gecht M, Bagola K, Horner C, et al. In situ structural analysis of SARS-CoV-2 spike reveals flexibility mediated by three hinges. *Sci*. 2020;370(6513):203–08. doi:10.1126/science.abd5223.
- Wrapp D, Wang N, Corbett KS, Goldsmith JA, Hsieh CL, Abiona O, Graham BS, McLellan JS. Cryo-EM structure of the 2019-nCoV spike in the prefusion conformation. *Sci*. 2020;367(6483):1260–63. doi:10.1126/science.abb2507.
- Shang J, Ye G, Shi K, Wan Y, Luo C, Aihara H, Geng Q, Auerbach A, Li F. Structural basis of receptor recognition by SARS-CoV-2. *Nat*. 2020;581(7807):221–24. doi:10.1038/s41586-020-2179-y.
- Andreano E, Nicastrì E, Paciello I, Pileri P, Manganaro N, Piccini G, Manenti A, Pantano E, Kabanova A, Troisi M, et al. Extremely potent human monoclonal antibodies from COVID-19 convalescent patients. *Cell*. 2021;184(7):1821–35 e16. doi:10.1016/j.cell.2021.02.035.
- Piccoli L, Park YJ, Tortorici MA, Czudnochowski N, Walls AC, Beltramello M, Silacci-Fregni C, Pinto D, Rosen LE, Bowen JE, et al. Mapping neutralizing and immunodominant sites on the SARS-CoV-2 spike receptor-binding domain by structure-guided high-resolution serology. *Cell*. 2020;183(4):1024–42 e21. doi:10.1016/j.cell.2020.09.037.
- Baum A, Ajithdoss D, Copin R, Zhou A, Lanza K, Negron N, Ni M, Wei Y, Mohammadi K, Musser B, et al. REGN-COV2 antibodies prevent and treat SARS-CoV-2 infection in rhesus macaques and hamsters. *Sci*. 2020;370(6520):1110–15. doi:10.1126/science.abe2402.

11. Cathcart AL, Havenar-Daughton C, Lempp FA, Ma D, Schmid MA, Agostini ML, Guarino B, Di Iulio J, Rosen LE, Tucker H, et al. The dual function monoclonal antibodies VIR-7831 and VIR-7832 demonstrate potent in vitro and in vivo activity against SARS-CoV-2. *bioRxiv* 2021:2021.03.09.434607. doi:10.1101/2021.03.09.434607
12. Gottlieb RL, Nirula A, Chen P, Boscia J, Heller B, Morris J, Huhn G, Cardona J, Mocherla B, Stosor V, et al. Effect of bamlanivimab as monotherapy or in combination with etesevimab on viral load in patients with mild to moderate COVID-19: a randomized clinical trial. *JAMA*. 2021;325(7):632–44. doi:10.1001/jama.2021.0202.
13. Hansen J, Baum A, Pascal KE, Russo V, Giordano S, Wloga E, Fulton BO, Yan Y, Koon K, Patel K, et al. Studies in humanized mice and convalescent humans yield a SARS-CoV-2 antibody cocktail. *Sci*. 2020;369(6506):1010–14. doi:10.1126/science.abd0827.
14. Zost SJ, Gilchuk P, Case JB, Binshtein E, Chen RE, Nkolola JP, Schafer A, Reidy JX, Trivette A, Nargi RS, et al. Potently neutralizing and protective human antibodies against SARS-CoV-2. *Nat*. 2020;584(7821):443–49. doi:10.1038/s41586-020-2548-6.
15. Cherian S, Potdar V, Jadhav S, Yadav P, Gupta N, Das M, Rakshit P, Singh S, Abraham P, Panda S. Convergent evolution of SARS-CoV-2 spike mutations. L452R, E484Q and P681R, in the second wave of COVID-19 in Maharashtra. *India: bioRxiv* 2021:2021.04.22.440932. doi:10.1101/2021.04.22.440932
16. Davies NG, Abbott S, Barnard RC, Jarvis CI, Kucharski AJ, Munday JD, Pearson CAB, Russell TW, Tully DC, Washburne AD, et al. Estimated transmissibility and impact of SARS-CoV-2 lineage B.1.1.7 in England. *Sci*. 2021;373(6553):372. doi:10.1126/science.abg3055.
17. Tegally H, Wilkinson E, Giovanetti M, Iranzadeh A, Fonseca V, Giandhari J, Doolabh D, Pillay S, San EJ, Msomi N, et al. Emergence and rapid spread of a new severe acute respiratory syndrome-related coronavirus 2 (SARS-CoV-2) lineage with multiple spike mutations in South Africa. *medRxiv* 2020:2020.12.21.20248640. doi:10.1101/2020.12.21.20248640
18. Volz E, Mishra S, Chand M, Barrett JC, Johnson R, Geidelberg L, Hinsley WR, Laydon DJ, Dabrera G, O’Toole Á, et al. Transmission of SARS-CoV-2 lineage B.1.1.7 in England: insights from linking epidemiological and genetic data. *medRxiv* 2021:2020.12.30.20249034. doi:10.1101/2020.12.30.20249034
19. Wilhelm A, Widera M, Grikscheit K, Toptan T, Schenk B, Pallas C, Metzler M, Kohmer N, Hoehl S, Helfritz FA, et al. Reduced neutralization of SARS-CoV-2 omicron variant by vaccine sera and monoclonal antibodies. *medRxiv* 2021:2021.12.07.21267432. doi:10.1101/2021.12.07.21267432
20. Cameroni E, Bowen JE, Rosen LE, Saliba C, Zepeda SK, Culap K, Pinto D, VanBlargan LA, De Marco A, Di Iulio J, et al. Broadly neutralizing antibodies overcome SARS-CoV-2 Omicron antigenic shift. *Nat*. 2022;602(7898):664–70. doi:10.1038/s41586-021-04386-2.
21. Cao YR, Wang J, Jian F, Xiao T, Song W, Yisimayi A, Huang W, Li Q, Wang P, An R, et al. Omicron escapes the majority of existing SARS-CoV-2 neutralizing antibodies. *bioRxiv* 2021:2021.12.07.470392. doi:10.1101/2021.12.07.470392.
22. Iketani S, Liu L, Guo Y, Liu L, Chan JF, Huang Y, Wang M, Luo Y, Yu J, Chu H, et al. Antibody evasion properties of SARS-CoV-2 Omicron sublineages. *Nat*. 2022;604(7906):553–56. doi:10.1038/s41586-022-04594-4.
23. Onodera T, Kita S, Adachi Y, Moriyama S, Sato A, Nomura T, Sakakibara S, Inoue T, Tadokoro T, Anraku Y, et al. A SARS-CoV-2 antibody broadly neutralizes SARS-related coronaviruses and variants by coordinated recognition of a virus-vulnerable site. *Immunity*. 2021;54(10):2385–2398.e10. doi:10.1016/j.immuni.2021.08.025.
24. Starr TN, Czudnochowski N, Liu Z, Zatta F, Park YJ, Addetia A, Pinto D, Beltramello M, Hernandez P, Greaney AJ, et al. SARS-CoV-2 RBD antibodies that maximize breadth and resistance to escape. *Nat*. 2021;597(7874):97–102. doi:10.1038/s41586-021-03807-6.
25. Tortorici MA, Czudnochowski N, Starr TN, Marzi R, Walls AC, Zatta F, Bowen JE, Jaconi S, Di Iulio J, Wang Z, et al. Broad sarbecovirus neutralization by a human monoclonal antibody. *Nat*. 2021;597(7874):103–08. doi:10.1038/s41586-021-03817-4.
26. Tani H, Kimura M, Tan L, Yoshida Y, Ozawa T, Kishi H, Fukushi S, Saijo M, Sano K, Suzuki T, et al. Evaluation of SARS-CoV-2 neutralizing antibodies using a vesicular stomatitis virus possessing SARS-CoV-2 spike protein. *Virol J*. 2021;18(1):16. doi:10.1186/s12985-021-01490-7.
27. Jin A, Ozawa T, Tajiri K, Obata T, Kishi H, Muraguchi A. Rapid isolation of antigen-specific antibody-secreting cells using a chip-based immunospot array. *Nat Protoc*. 2011;6(5):668–76. doi:10.1038/nprot.2011.322.
28. Jin A, Ozawa T, Tajiri K, Obata T, Kondo S, Kinoshita K, Kadowaki S, Takahashi K, Sugiyama T, Kishi H, et al. A rapid and efficient single-cell manipulation method for screening antigen-specific antibody-secreting cells from human peripheral blood. *Nat Med*. 2009;15(9):1088–92. doi:10.1038/nm.1966.
29. Yamada H, Sasaki S, Tani H, Somekawa M, Kawasuji H, Saga Y, Yoshida Y, Yamamoto Y, Hayakawa Y, Morinaga Y. A novel hamster model of SARS-CoV-2 respiratory infection using a pseudotyped virus. *bioRxiv* 2021:2021.09.17.460745. doi:10.1101/2021.09.17.460745
30. Robbiani DF, Gaebler C, Muecksch F, Lorenzi JCC, Wang Z, Cho A, Agudelo M, Barnes CO, Gazumyan A, Finkin S, et al. Convergent antibody responses to SARS-CoV-2 in convalescent individuals. *Nat*. 2020;584(7821):437–42. doi:10.1038/s41586-020-2456-9.
31. Yuan M, Liu H, Wu NC, Lee CD, Zhu X, Zhao F, Huang D, Yu W, Hua Y, Tien H, et al. Structural basis of a shared antibody response to SARS-CoV-2. *Sci*. 2020;369:1119–23. doi:10.1126/science.abd2321.
32. Dong J, Zost SJ, Greaney AJ, Starr TN, Dingens AS, Chen EC, Chen RE, Case JB, Sutton RE, Gilchuk P, et al. Genetic and structural basis for SARS-CoV-2 variant neutralization by a two-antibody cocktail. *Nat Microbiol*. 2021;6(10):1233–44. doi:10.1038/s41564-021-00972-2.
33. Tortorici MA, Beltramello M, Lempp FA, Pinto D, Dang HV, Rosen LE, McCallum M, Bowen J, Minola A, Jaconi S, et al. Ultrapotent human antibodies protect against SARS-CoV-2 challenge via multiple mechanisms. *Sci*. 2020;370(6519):950–57. doi:10.1126/science.abe3354.
34. Dejnirattisai W, Zhou D, Ginn HM, Duyvesteyn HME, Supasa P, Case JB, Zhao Y, Walter TS, Mentzer AJ, Liu C, et al. The antigenic anatomy of SARS-CoV-2 receptor binding domain. *Cell*. 2021;184(8):2183–200 e22. doi:10.1016/j.cell.2021.02.032.
35. Wang L, Zhou T, Zhang Y, Yang ES, Schramm CA, Shi W, Pegu A, Oloniniyi OK, Henry AR, Darko S, et al. Ultrapotent antibodies against diverse and highly transmissible SARS-CoV-2 variants. *Sci*. 2021;373(6553):373. doi:10.1126/science.abh1766.
36. Brouwer PJM, Caniels TG, van der Straten K, Snitselaar JL, Aldon Y, Bangaru S, Torres JL, Okba NMA, Claireaux M, Kerster G, et al. Potent neutralizing antibodies from COVID-19 patients define multiple targets of vulnerability. *Sci*. 2020;369(6504):643–50. doi:10.1126/science.abc5902.
37. Sui J, Hwang WC, Perez S, Wei G, Aird D, Chen LM, Santelli E, Stec B, Cadwell G, Ali M, et al. Structural and functional bases for broad-spectrum neutralization of avian and human influenza A viruses. *Nat Struct Mol Biol*. 2009;16(3):265–73. doi:10.1038/nsmb.1566.
38. Wheatley AK, Whittle JR, Lingwood D, Kanekiyo M, Yassine HM, Ma SS, Narpala SR, Prabhakaran MS, Matus-Nicodemus RA, Bailer RT, et al. H5N1 vaccine-elicited memory B cells are genetically constrained by the IGHV locus in the recognition of a neutralizing epitope in the hemagglutinin stem. *J Immunol*. 2015;195(2):602–10. doi:10.4049/jimmunol.1402835.

39. Kreer C, Zehner M, Weber T, Ercanoglu MS, Gieselmann L, Rohde C, Halwe S, Korenkov M, Schommers P, Vanshylla K, et al. Longitudinal isolation of potent near-germline SARS-CoV-2-neutralizing antibodies from COVID-19 patients. *Cell*. 2020;182(4):843–54 e12. doi:10.1016/j.cell.2020.06.044.
40. Schmitz AJ, Turner JS, Liu Z, Aziati ID, Chen RE, Joshi A, Bricker TL, Darling TL, Adelsberg DC, Alsoussi WB, et al. A public vaccine-induced human antibody protects against SARS-CoV-2 and emerging variants. *bioRxiv* 2021:2021.03.24.436864. doi:10.1101/2021.03.24.436864
41. Wang Z, Schmidt F, Weisblum Y, Muecksch F, Barnes CO, Finkin S, Schaefer-Babajew D, Cipolla M, Gaebler C, Lieberman JA, et al. mRNA vaccine-elicited antibodies to SARS-CoV-2 and circulating variants. *Nat*. 2021. doi:10.1038/s41586-021-03324-6.
42. Pan R, Qin Y, Banasik M, Lees W, Shepherd AJ, Cho MW, Kong XP. Increased epitope complexity correlated with antibody affinity maturation and a novel binding mode revealed by structures of rabbit antibodies against the third variable loop (V3) of HIV-1 gp120. *J Virol*. 2018;92. doi:10.1128/JVI.01894-17.
43. Qin Y, Banerjee S, Agrawal A, Shi H, Banasik M, Lin F, Rohl K, LaBranche C, Montefiori DC, Cho MW. Characterization of a large panel of rabbit monoclonal antibodies against HIV-1 gp120 and isolation of novel neutralizing antibodies against the V3 loop. *PLoS One*. 2015;10(6):e0128823. doi:10.1371/journal.pone.0128823.
44. Lan J, Ge J, Yu J, Shan S, Zhou H, Fan S, Zhang Q, Shi X, Wang Q, Zhang L, et al. Structure of the SARS-CoV-2 spike receptor-binding domain bound to the ACE2 receptor. *Nat*. 2020;581(7807):215–20. doi:10.1038/s41586-020-2180-5.
45. Yan R, Zhang Y, Li Y, Xia L, Guo Y, Zhou Q. Structural basis for the recognition of SARS-CoV-2 by full-length human ACE2. *Sci*. 2020;367(6485):1444–48. doi:10.1126/science.abb2762.
46. Yi C, Sun X, Ye J, Ding L, Liu M, Yang Z, Lu X, Zhang Y, Ma L, Gu W, et al. Key residues of the receptor binding motif in the spike protein of SARS-CoV-2 that interact with ACE2 and neutralizing antibodies. *Cell Mol Immunol*. 2020;17(6):621–30. doi:10.1038/s41423-020-0458-z.
47. Zhang X, Zheng M, Liang T, Zhou H, Wang H, Zhang J, Ren J, Peng H, Li S, Bian H, et al. Inhibitor screening of spike variants reveals the heterogeneity of neutralizing antibodies to COVID-19 infection and vaccination. *medRxiv* 2021:2021.05.15.21257254. doi:10.1101/2021.05.15.21257254
48. Prabakaran P, Chowdhury PS. Landscape of non-canonical cysteines in human VH repertoire revealed by immunogenetic analysis. *Cell Rep*. 2020;31(13):107831. doi:10.1016/j.celrep.2020.107831.
49. Morinaga Y, Tani H, Terasaki Y, Nomura S, Kawasuji H, Shimada T, Igarashi E, Saga Y, Yoshida Y, Yasukochi R, et al. Correlation of the commercial anti-SARS-CoV-2 receptor binding domain antibody test with the chemiluminescent reduction neutralizing test and possible detection of antibodies to emerging variants. *Microbiol Spectr*. 2021;9(3):e0056021. doi:10.1128/Spectrum.00560-21.
50. Tani H, Shiokawa M, Kaname Y, Kambara H, Mori Y, Abe T, Moriishi K, Matsuura Y. Involvement of ceramide in the propagation of Japanese encephalitis virus. *J Virol*. 2010;84(6):2798–807. doi:10.1128/JVI.02499-09.
51. Zaimoku Y, Takamatsu H, Hosomichi K, Ozawa T, Nakagawa N, Imi T, Maruyama H, Katagiri T, Kishi H, Tajima A, et al. Identification of an HLA class I allele closely involved in the autoantigen presentation in acquired aplastic anemia. *Blood*. 2017;129(21):2908–16. doi:10.1182/blood-2016-11-752378.
52. Ozawa T, Ouhara K, Tsuda R, Munenaga S, Kurihara H, Kohno H, Hamana H, Kobayashi E, Taki H, Tobe K, et al. Physiologic target, molecular evolution, and pathogenic functions of a monoclonal anti-citrullinated protein antibody obtained from a patient with rheumatoid arthritis. *Arthritis Rheumatol*. 2020;72(12):2040–49. doi:10.1002/art.41426.
53. Ozawa T, Masaki H, Takasaki T, Aoyama I, Yumisashi T, Yamanaka A, Konishi E, Ohnuki Y, Muraguchi A, Kishi H. Human monoclonal antibodies against West Nile virus from Japanese encephalitis-vaccinated volunteers. *Antiviral Res*. 2018;154:58–65. doi:10.1016/j.antiviral.2018.04.011.
54. Brochet X, Lefranc MP, Giudicelli V. IGM/V-QUEST: the highly customized and integrated system for IG and TR standardized V-J and V-D-J sequence analysis. *Nucleic Acids Res*. 2008;36(Web Server):W503–8. doi:10.1093/nar/gkn316.
55. Evans P. Scaling and assessment of data quality. *Acta Crystallogr D Biol Crystallogr*. 2006;62(1):72–82. doi:10.1107/S0907444905036693.
56. Kabsch W. Xds. *Acta Crystallogr D Biol Crystallogr*. 2010;66(2):125–32. doi:10.1107/S0907444909047337.
57. Winn MD, Ballard CC, Cowtan KD, Dodson EJ, Emsley P, Evans PR, Keegan RM, Krissinel EB, Leslie AG, McCoy A, et al. Overview of the CCP 4 suite and current developments. *Acta Crystallogr D Biol Crystallogr*. 2011;67(4):235–42. doi:10.1107/S0907444910045749.
58. Emsley P, Lohkamp B, Scott WG, Cowtan K. Features and development of coot. *Acta Crystallogr D Biol Crystallogr*. 2010;66(4):486–501. doi:10.1107/S0907444910007493.
59. Liebschner D, Afonine PV, Baker ML, Bunkoczi G, Chen VB, Croll TI, Hintze B, Hung LW, Jain S, McCoy AJ, et al. Macromolecular structure determination using X-rays, neutrons and electrons: recent developments in Phenix. *Acta Crystallogr D Struct Biol*. 2019;75(10):861–77. doi:10.1107/S2059798319011471.
60. Davis IW, Leaver-Fay A, Chen VB, Block JN, Kapral GJ, Wang X, Murray LW, Arendall WB 3rd, Snoeyink J, Richardson JS, et al. MolProbity: all-atom contacts and structure validation for proteins and nucleic acids. *Nucleic Acids Res*. 2007;35(Web Server):W375–83. doi:10.1093/nar/gkm216.
61. Krissinel E, Henrick K. Inference of macromolecular assemblies from crystalline state. *J Mol Biol*. 2007;372(3):774–97. doi:10.1016/j.jmb.2007.05.022.
62. Scheres SH. RELION: implementation of a bayesian approach to cryo-EM structure determination. *J Struct Biol*. 2012;180(3):519–30. doi:10.1016/j.jsb.2012.09.006.
63. Zivanov J, Nakane T, Forsberg BO, Kimanius D, Hagen WJ, Lindahl E, Scheres SH. New tools for automated high-resolution cryo-EM structure determination in RELION-3. *Elife*. 2018;7. doi:10.7554/eLife.42166.
64. Zheng SQ, Palovcak E, Armache JP, Verba KA, Cheng Y, Agard DA. MotionCorr2: anisotropic correction of beam-induced motion for improved cryo-electron microscopy. *Nat Methods*. 2017;14(4):331–32. doi:10.1038/nmeth.4193.
65. Rohou A, Grigorieff N. CTFFIND4: fast and accurate defocus estimation from electron micrographs. *J Struct Biol*. 2015;192(2):216–21. doi:10.1016/j.jsb.2015.08.008.
66. Pettersen EF, Goddard TD, Huang CC, Couch GS, Greenblatt DM, Meng EC, Ferrin TE. UCSF Chimera—a visualization system for exploratory research and analysis. *J Comput Chem*. 2004;25(13):1605–12. doi:10.1002/jcc.20084.
67. Itokawa K, Sekizuka T, Hashino M, Tanaka R, Kuroda M. Disentangling primer interactions improves SARS-CoV-2 genome sequencing by multiplex tiling PCR. *PLoS One*. 2020;15(9):e0239403. doi:10.1371/journal.pone.0239403.
68. Li H, Durbin R. Fast and accurate short read alignment with burrows-wheeler transform. *Bioinformatics*. 2009;25(14):1754–60. doi:10.1093/bioinformatics/btp324.
69. Koboldt DC, Zhang Q, Larson DE, Shen D, McLellan MD, Lin L, Miller CA, Mardis ER, Ding L, Wilson RK. VarScan 2: somatic mutation and copy number alteration discovery in cancer by exome sequencing. *Genome Res*. 2012;22(3):568–76. doi:10.1101/gr.129684.111.
70. Melero R, Sorzano COS, Foster B, Vilas JL, Martinez M, Marabini R, Ramirez-Aportela E, Sanchez-Garcia R, Herreros D, Del Cano L, et al. Continuous flexibility analysis of SARS-CoV-2 spike prefusion structures. *IUCrJ*. 2020;7. doi:10.1107/S2052252520012725.